

GEMINI FOLLOW-UP OF TWO MASSIVE H I CLOUDS DISCOVERED WITH THE AUSTRALIAN SQUARE KILOMETER ARRAY PATHFINDER

JUAN P. MADRID¹, KAREN LEE-WADDELL¹, PAOLO SERRA^{1,2}, BÄRBEL S. KORIBALSKI¹, MISCHA SCHIRMER³, KRISTINE SPEKKENS⁴, JING WANG¹

Draft version February 16, 2018

ABSTRACT

Using the Gemini Multi Object Spectrograph (GMOS) we search for optical counterparts of two massive ($\sim 10^9 M_\odot$) neutral hydrogen clouds near the spiral galaxy IC 5270, located in the outskirts of the IC 1459 group. These two H I clouds were recently discovered using the Australian Square Kilometer Array Pathfinder (ASKAP). Two low surface brightness optical counterparts to one of these H I clouds are identified in the new Gemini data that reaches down to magnitudes of ~ 27.5 mag in the g -band. The observed H I mass to light ratio derived with these new data, $M_{H I}/L_g = 242$, is among the highest reported to date. We are also able to rule out that the two H I clouds are dwarf companions of IC 5270. Tidal interactions and ram pressure stripping are plausible explanations for the physical origin of these two clouds.

Subject headings: Galaxies: evolution — galaxies: individual (IC 5270) — galaxies: groups: individual (IC 1459) — stars: formation

1. INTRODUCTION

In the standard hierarchical clustering model of galaxy formation large structures form from the accretion and merger of small dark matter halos (White & Rees 1978). One of the main challenges of the Λ CDM model is the prediction of a large number of dark matter halos and satellite galaxies that remain observationally undetected. This limitation of the hierarchical clustering model could be solved by the detection of halos where star formation has been truncated so they remain optically faint but detectable through neutral hydrogen (H I) emission (e.g. Bonamente et al. 2008).

Despite the impact that observations of pure H I proto-galaxies would have on cosmology, such detections remain rare. The main all-sky surveys of neutral hydrogen such as the H I Parkes All Sky Survey (HIPASS; Koribalski et al. 2004; Meyer et al. 2015) and the Arecibo Legacy Fast ALFA (ALFALFA; Haynes et al. 2011) have found few examples of massive H I detections without optical counterparts.

Among the 1000 H I-brightest HIPASS sources (Koribalski et al. 2004) HIPASS J0731–69 stands out as the only extragalactic source without a clear optical counterpart. HIPASS J0731–69, however, has a clear link with NGC 2442, a spiral galaxy with asymmetric spiral arms and disturbed morphology located in the NGC 2434 group. The H I reservoir that constitutes HIPASS J0731–69 was most likely dislodged from NGC 2442 during a recent tidal encounter (Bekki et al. 2005).

In the northern hemisphere, of the 15,855 sources detected by the 40% ALFALFA catalog only 1.5% lack

survey-grade optical counterparts (Haynes et al. 2011; Cannon et al. 2015). Out of the 15,855 sources of the 40% ALFALFA catalog 15,041 of them are extragalactic. Recent observing campaigns targeting H I sources without optical counterparts in the ALFALFA survey have revealed ultra-low surface brightness structures, tidal dwarf galaxies and objects with exceptionally high mass-to-light ratio (Lee-Waddell et al. 2014; Janowiecki et al. 2015; Cannon et al. 2015).

Other intergalactic H I clouds without clear optical counterparts have also been discovered outside the main all sky surveys. For instance, Osterloo & van Gorkom (2005) report a large H I tail ($3.4 \times 10^8 M_\odot$) near the center of the Virgo cluster. The origin of this cloud is likely ram pressure stripping of NGC 4388 by M 86. Another example of intergalactic H I, also in Virgo, is H I 1225+01 (Giovanelli & Haynes 1989; Chengalur et al. 1995). H I 1225+01 has two main components separated by 100 kpc with H I masses of $10^9 M_\odot$. One of the two components is associated with a low surface brightness galaxy while the second component does not have an identified optical counterpart (Matsuoka et al. 2012). See also the example of the Vela cloud, a large and massive intergalactic H I cloud residing in the NGC 3256 group (English et al. 2010).

The Leo Triplet (NGC 3623, NGC 3627, and NGC 3628) is the classical example of a large tail of neutral hydrogen (Haynes et al. 1979) where a faint tidal tail of stars, coincidental with the H I peaks, was discovered with deep optical follow-up (Chromey et al. 1998).

Similarly, in this paper, we use new deep Gemini images to search for the first signs of star formation within two massive H I clouds recently discovered near the spiral galaxy IC 5270. The two H I clouds that are the target of this study have neutral hydrogen masses comparable to the Milky Way's.

2. ASKAP OBSERVATIONS OF THE IC 1459 GROUP BY SERRA ET AL. (2015)

¹ CSIRO Astronomy and Space Science, PO BOX 76, Epping NSW 1710, Australia

² Osservatorio Astronomico di Cagliari, Istituto Nazionale di Astrofisica, Italy

³ Gemini Observatory, Southern Operations Center, Colina El Pino s/n, La Serena, Chile

⁴ Department of Physics, Royal Military College of Canada, PO Box 17000, Station Forces, Kingston ON K7K 7B4, Canada

TABLE 1
SUMMARY OF OBSERVATIONAL PROPERTIES

Target Cloud	R.A.	Dec	H I mass (M_{\odot})	Observing Date	IQ	Cloud Cover	Total exposure time (s)
(1)	(2)	(3)	(4)	(5)	(6)	(7)	(8)
North	22:57:54.64	-35:47:59.1	$1.6 \pm 0.4 \times 10^9$	2016 Aug 04	85%	50%	3000
North East	22:57:54.64	-35:47:59.1	$1.0 \pm 0.2 \times 10^9$	2016 Aug 02	70-85%	50%	2200

NOTE. — Column (1): Target cloud; Column (2) and (3): R.A. and Dec of peak H I intensity; Column (4): H I mass in solar masses; Column (5) Observing Date; Column (6): Image quality in percentile; Column (7): Cloud cover in percentile; Column (8): Total exposure time in seconds.

The recent analysis of early commissioning data obtained with the Australian Square Kilometer Array Pathfinder (ASKAP) revealed the existence of three galaxy-size clouds of neutral hydrogen in the galaxy group IC 1459 without any documented optical emission (Serra et al. 2015). One of these clouds is linked to NGC 7418 while the two other clouds, which are the target of this study, are located near IC 5270. Each of these two large H I accumulations have the characteristic H I mass of galaxies ($\sim 10^9 M_{\odot}$) but, intriguingly, have no optical counterpart in the Digital Sky Survey – see Figure 1, top panel.

The galaxy group IC 1459 is located at a distance of 29 Mpc (Blakeslee et al. 2001) and is named after its brightest ($m_B = 11.0$ mag), early type member.

The 11 ASKAP detections with optical counterparts in this galaxy group span a range of H I masses from $5.4 \times 10^9 M_{\odot}$ down to $0.5 \times 10^9 M_{\odot}$. The two H I clouds we follow up with the Gemini telescope stand out as they are more massive in H I than several of the other detections in IC 1459 which have bright optical counterparts.

The H I emission associated with IC 5270 has a heliocentric velocity of $v_{hel} \sim 1790 - 2110$ km/s in the ASKAP spectra obtained by Serra et al. (2015), in agreement with the optical redshift of 1858 km/s (Da Costa et al. 1998). The two H I clouds have emission at radial velocities of $v_{hel} \sim 1900 - 2110$ km/s. The HIPASS data of this system shows that IC 5270 and the two neighbouring hydrogen clouds are linked by a diffuse and extended H I envelope.

The largest of the two clouds (North cloud) has a slight velocity gradient in H I – Serra et al. (2015), their figure 6. The second, lighter, North-East cloud has a far more homogeneous velocity field (moment-one) in the ASKAP data. The HIPASS name for the IC 5270 system (galaxy + clouds) is HIPASS J2258–35.

3. GEMINI OBSERVATIONS AND DATA REDUCTION

We obtained deep g -band images of these two H I clouds with the Gemini Multi Object Spectrograph (GMOS) on Gemini South under program GS-2016B-Q-61. Imaging in the g -band (475 nm) was chosen given that this filter is sensitive to both old and new stellar populations (e.g. Lee-Waddell et al. 2014). GMOS was used with 2×2 binning, resulting in a plate scale of $0.16''$ pixel $^{-1}$.

The two targets were observed on 2016 August 02 and 2016 August 04 under photometric conditions (Cloud Cover 50th percentile). Importantly for our science objectives, all observations were obtained with the dark-

est sky conditions (Surface Brightness 20th percentile). These observing conditions are optimal to detect extended low-surface brightness objects in g -band. The seeing ranged between $0.9''$ and $1.5''$, resulting in an effective image seeing in the coadded image of $1.1''$. Fourteen exposures of 200 s were obtained for the North cloud, and eleven exposures of the North-Eastern cloud.

A $20''$ wide dither pattern was chosen to cover the gaps between the three GMOS detectors, and the two GMOS pointings overlap so that we could image a continuous field over the area of the H I detections. A summary of the observations is given in Table 1.

Data were reduced with the THELI pipeline (Schirmer 2013; Erben et al. 2005) following standard procedures. Exposures were overscan corrected, bias subtracted, and flat fielded using twilight exposures. Individual weight maps were created to mask cosmic rays and other detector defects. For the astrometric calibration, THELI uses `Scamp` (Bertin & Arnouts 1996). Source catalogs (mostly stars) were extracted from the images and matched against the Initial Gaia Source List (IGSL, Smart & Nicastro 2014) in the J2000 ICRF reference frame. Images were distortion-corrected using a third-order polynomial description, and registered with respect to each other with a typical precision of 1/20th pixel.

Accurate, yet conservative background correction of individual exposures is crucial for the detection of extended low-surface brightness objects. Background subtraction was carried out several times and with different parameters in order to ensure that faint structures both small and large were detectable. THELI uses `SExtractor` (Bertin & Arnouts 1996) to detect and mask objects in the field; `SExtractor` was configured with a detection threshold of 1.5σ and a minimum number of 10 connected pixels above the detection threshold. The size of the object masks was extended by a factor of three (see Schirmer et al. 2015) to include hidden flux around faint objects. The images that we present in Figures 1 and 2, were created using the masks described above that were then convolved with a FWHM = 400 pixel wide ($1.1'$ Gaussian kernel, and the resulting background models were subtracted. For the data reduction presented in Figures 1 and 2 all potential structures with an angular extent of less than $\sim 1'$ (8 kpc physical scale) are preserved. Several trials of background subtraction with different parameters were carried out to ensure that very faint structures of all sizes and with fluxes similar to the background level were preserved.

At the distance of IC 5270 (29 Mpc) one arcsecond corresponds to a physical scale of 137 pc (Wright 2006).

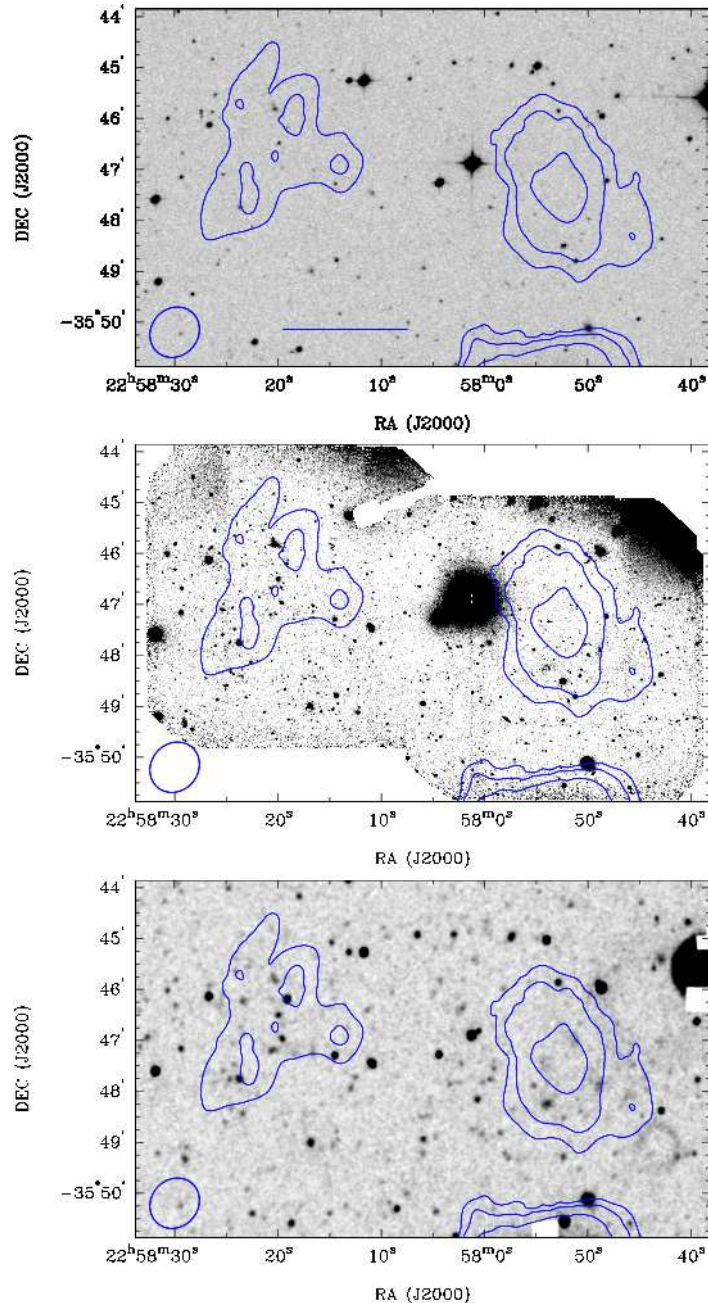


FIG. 1.— *Top panel:* Blue ASKAP contours of the two H I clouds located North and North-East of IC 5270 overlaid on a Digital Sky Survey (red) image. The contours visible on the lower right hand corner are those of IC 5270. The physical size of this image is $\sim 50 \times 85$ kpc, the scale bar represents ~ 20 kpc. North is up and east is left. The radial velocity range of the H I emission is $v_{hel} \sim 1900 - 2110$ km/s. *Middle panel:* Mosaic of the Gemini GMOS g -band images of the same area of the sky as the above panel. The vignetting is due to the placement of the On Instrument Wavefront Sensor (OIWFS) on a guide star within the science field. *Bottom panel:* Archival Near-Ultraviolet GALEX image. This GALEX image was smoothed by a Gaussian kernel of 2 pixels.

The GMOS field of view of 5.5×5.5 arcmin² thus corresponds to an area of $\sim 45.2 \times 45.2$ kpc². On our coadded image we can see structures of 150 pc at the distance of IC 5270, significantly smaller than typical Tidal Dwarf Galaxies (Lee-Waddell et al. 2016). A mosaic of the two fields imaged with GMOS is presented in Figure 1 – middle panel.

4. RESULTS

The most evident result, clearly visible in Figure 1, is the lack of both large diffuse optical counterparts and

of stellar streams in the field of the two H I clouds. The new Gemini data, while deep enough to reveal the presence of stellar tidal tails, like the ones found by Lee-Waddell et al. (2012), is free of such large scale features. With the Gemini images we detect the faint outer isophotes of the IC 5270 disk but no tidal disturbance is found on the northern part of this galaxy. We are also able to rule out that the two H I clouds are dwarf companions of IC 5270.

On the Gemini images we identify two ultra-faint optical counterparts to the North Cloud. The overall mor-

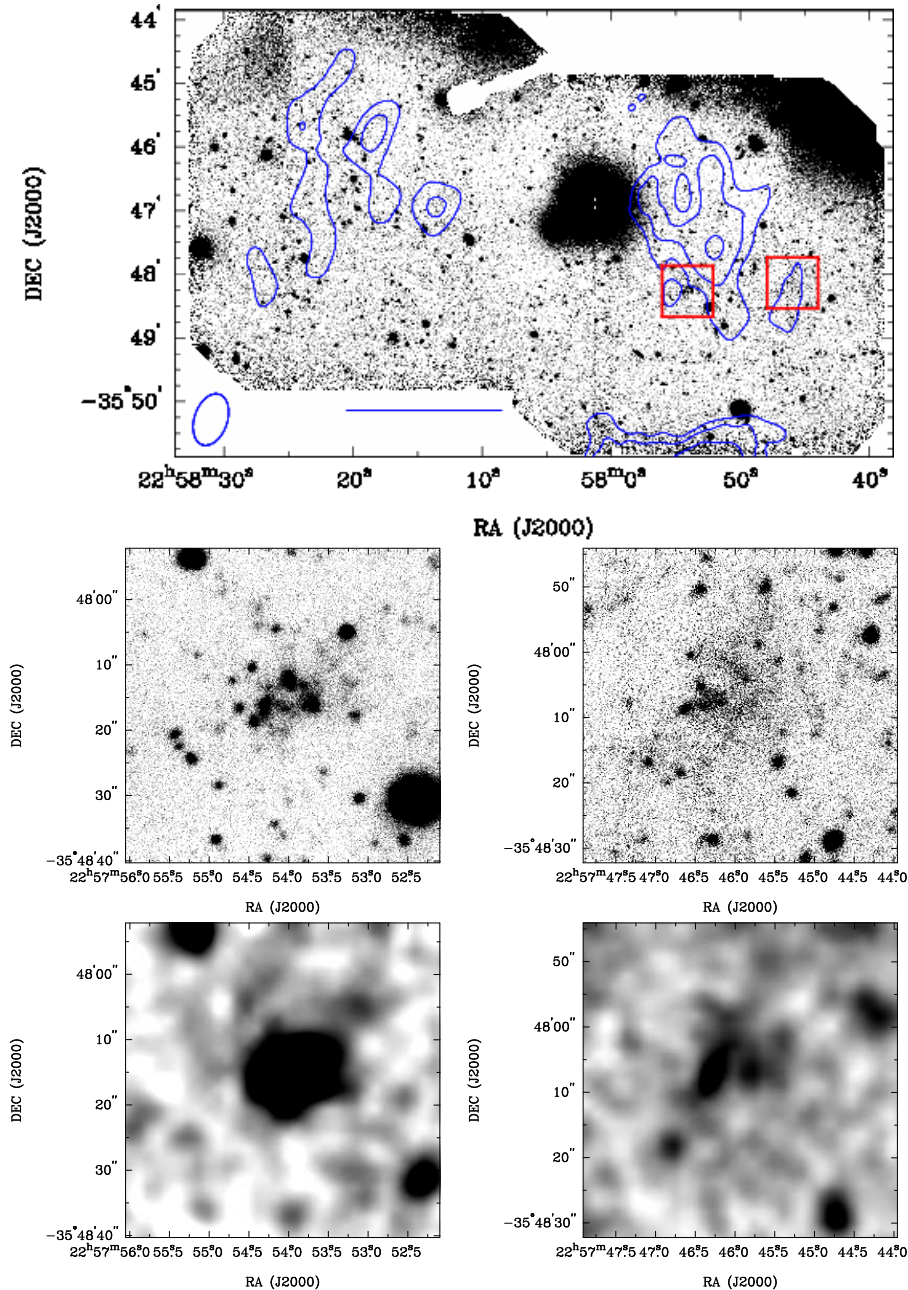


FIG. 2.— *Top panel:* New Gemini image with ASKAP contours obtained with the new data reduction presented here which trace the regions with the highest H I column densities. The highest column density on the North cloud is $N_H = 1.4 \times 10^{21} \text{cm}^{-2}$ while its outer contours trace column densities of $N_H \sim 0.5 \times 10^{21} \text{cm}^{-2}$. The highest column density of the North-East cloud is $N_H = 0.7 \times 10^{21} \text{cm}^{-2}$. The red boxes show the location of the two optical counterparts. The scale bar represents ~ 20 kpc. *Middle panel left:* Zoom of the Gemini image of the western optical counterpart (ID 1 on Table 2). *Middle panel right:* Zoom of the Gemini image of the eastern optical counterpart (ID 2 on Table 2). *Bottom panel left:* Zoom of the GALEX image of the eastern optical counterpart (ID 1 on Table 2). *Bottom panel right:* Zoom of the GALEX image of the eastern optical counterpart (ID 2 on Table 2). The archival GALEX image has an exposure time of 3306 seconds and was observed in 2010 October 31.

phology of these objects is similar to the sources recently presented by Leisman et al. (2017). That is, clusters of clumps associated with ultra-diffuse emission. Moreover, these sources also have detectable flux in Near Ultraviolet (NUV) archival images obtained by GALEX. The NUV is a very sensitive tracer of recent star formation. The location of these ultra-low surface brightness structures is highlighted on the top panel of Figure 2 with two red boxes. A zoom on these sources is shown in Figure 2 where the new Gemini images (middle panels) are

presented alongside the archival GALEX images (bottom panels).

The top panel of Fig. 2 shows the new Gemini image and the H I contours of a new data reduction of the ASKAP data. The new data reduction of the radio data was carried out giving more weight to longer baselines and improving our resolution, that is, using $\text{robust} = 0$. For the $\text{robust} = 0$ weighting the PSF is $48'' \times 35''$ and the peak H I brightness in the North cloud is $\sim 2.2 \text{ Jy beam}^{-1} \text{ km s}^{-1}$ which translates into

$N_H = 1.4 \times 10^{21} \text{cm}^{-2}$. This new data reduction was carried out in order to identify those regions with the highest H I column density, where star formation has the highest likelihood to occur.

With our new Gemini data we are able to detect sources down to g -band magnitudes of ~ 27.5 mag, at three sigma above the local background. By running **SExtractor** with a 3σ detection threshold on the deep Gemini images we detect ~ 1900 sources within the field of view. This is in contrast with the much shallower DSS image that appears virtually free of sources in the area of interest. Indeed, when we run **SExtractor** on the DSS image (top panel Fig. 1) only 128 sources are detected.

Two bright objects are easily identifiable within the H I contours of IC 5270. On the DSS and GALEX images these two objects are the only ones present in the northern edge of IC 5270. The brightest object (RA=22:57:49.94, Dec=-35:50:07.9) reveals itself as a background face-on spiral on the Gemini data. The second object (RA=22:57:52.29, Dec=-35:50:33.4) is ultra-compact and it is likely to be a background star-forming galaxy.

4.1. Photometry of faint optical counterparts

We carry out aperture photometry of the faint optical counterparts with the task `phot` within the `daophot` package in `PyRAF`. We measure the flux of the optical counterparts with an aperture of 35 and 70 pixels in radius, as a function of their respective sizes. The eastern source (ID 1 on Table 1) is indeed more compact than the source to the west (ID 2 on Table 1). We use a zeropoint of $ZP = 27.32$ mag to convert fluxes to g band magnitudes. We obtain $m_g = 21.3 \pm 0.25$ mag for the source on the left of Figure 2, middle panel (ID 1) and $m_g = 21.2 \pm 0.25$ mag for the other source (ID 2). By assuming that the neutral hydrogen clouds and the optical counterpart are at the same distance as IC 5270 (29 Mpc) we derive absolute magnitudes of $M_g = -11.01$ mag and $M_g = -11.15$.

By adopting the absolute magnitude of the Sun to be $M_{\odot,g} = 5.12$ mag (Sparke & Gallagher 2007) we can obtain the solar luminosity of the ultra faint optical counterparts of the North cloud to be $L = 3.1 \pm 0.6 \times 10^6 L_{\odot}$ and $L = 3.5 \pm 0.66 \times 10^6 L_{\odot}$. Properties of the ultra-faint and ultra-diffuse optical counterparts are summarized in Table 2.

4.2. An extremely high H I mass to stellar light ratio

With the absolute magnitudes obtained with the new Gemini data and the H I masses published by Serra et al. (2015) we can now derive an observed H I mass-to-light ratio:

$$\frac{M_{HI}}{L_g} = \frac{1.6 \times 10^9}{6.6 \times 10^6} = 242 \pm 76. \quad (1)$$

This gas-to-light ratio is higher than other extreme values recently published: Janowiecki et al. (2015) give a value of $M_{HI}/L_g > 57$ for the HI1232+20 system and Janesh et al. (2017) find an upper limit of 144 for the gas to light ratio of AGC 249525.

The North-East cloud lacks any obvious optical counterpart on our deep Gemini images. We derive a crude lower limit of the gas-to-light ratio for the North-East

TABLE 2
PROPERTIES OF OPTICAL COUNTERPARTS

ID	R.A.	Dec	Absolute g Magnitude	L_{\odot}
(1)	(2)	(3)	(4)	(5)
(1)	22:57:54.00	-35:48:15.6	-11.01	3.1×10^6
(2)	22:57:45.92	-35:48:04.7	-11.15	3.5×10^6

NOTE. — Column (1): Optical counterpart ID, counterpart with ID 1 is the easternmost object, counterpart with ID 2 is the westernmost one; Column (2): Right ascension; Column (3): Declination; Column (4): Absolute magnitude in g -band; Column (5): Equivalent solar luminosities.

cloud by assuming that any existing optical counterpart will be fainter than the faintest detection we present here:

$$\frac{M_{HI}}{L_g} = \frac{1.0 \times 10^9}{3.1 \times 10^6} > 322 \pm 101. \quad (2)$$

5. DISCUSSION

5.1. “Two missing galaxies problem”

As mentioned in the Introduction, the two neutral hydrogen clouds that we follow up with Gemini have similar H I content as the Milky Way. One possibility to explain the absence of two Milky-Way-sized galaxies cospatial with these clouds is their low H I column density. The surface density threshold for star formation is given by Schaye (2004) in terms of H I column density: $N_{H,crit} \sim (3-10) \times 10^{20} \text{cm}^{-2}$. This value is in agreement with the column density required to detect clustered star formation as given by Mullan et al. (2013).

The new data reduction carried out for this work shows that the maximum H I column density is above the expected critical threshold to trigger star formation. Given that relatively few stars are detected compared to the amount of available H I makes this system an extreme case of star formation inefficiency. However, the derived column density might be above the star formation threshold only in projection and the H I might be too diffuse to have significant star formation. Assuming a constant uniform distribution of H I in a $8 \times 8 \times 8$ kpc cube, the volume density of the brightest H I features would be 0.06cm^{-3} , within the range of the star formation threshold found by Schaye & Dalla Vecchia (2008): 0.01cm^{-3} to 0.1cm^{-3} but below higher values also commonly used (0.13cm^{-3} , e.g. Davé et al. 2017). Instead of a uniform distribution, the H I is more likely to form sheets, filaments and dense clumps where pockets of star formation can occur.

5.2. Origin of the H I clouds

From the analysis of ASKAP and HIPASS data Serra et al. (2015) concluded that the two massive H I clouds must be ‘the tip of the iceberg’ of a large scale distribution of H I gas that encompasses IC 5270.

Is the origin of these clouds the result of tidal interactions between IC 5270 and a nearby group member? As mentioned above, we detect the faint outer isophotes of the IC 5270 disk on the new Gemini images but no streams or tails are detected. An inspection of IC 5270

stellar morphology of IC 5270 reveals that this galaxy has smooth isophotes. The surface brightness profile of IC 5270 in the DSS2 red filter is smooth and it is well fit by a single Sérsic model. The DSS2 blue filter shows a central component on the surface brightness profile that is likely due to star formation. In any event, the optical data available for IC 5270 show no signs of strong tidal interactions. However, mild tidal interactions between group members can create starless H I tails by removing gas-rich material from the outskirts of disk galaxies (Bekki et al. 2005) without affecting the distribution of stars. The large number of H I ‘debris’ present within the IC 1459 galaxy group are signposts of rich interactions between group members (Saponara et al. 2018).

Ram pressure stripping by the intergroup medium offers another plausible explanation for the origin of these two clouds. Indeed, ram pressure stripping can remove gas from galaxies that are either not tidally interacting or experiencing weak tidal interactions (Hester 2006). Ram pressure could have dislodged the H I material that constitutes these two clouds from the outskirts of IC 5270 without altering its stellar structure. Limitations to the ram pressure hypothesis are the facts that the IC 1459 is a group with low velocity dispersion $\sigma = 223 \pm 62$ km/s (Osmond & Ponman 2004) and IC 5270 is more than 400

kpc from the group center.

Based on observations obtained at the Gemini Observatory which is operated by the AURA under a cooperative agreement with the NSF on behalf of the Gemini partnership.

The Australian SKA Pathfinder is part of the Australia Telescope National Facility which is managed by CSIRO. Operation of ASKAP is funded by the Australian Government with support from the National Collaborative Research Infrastructure Strategy. ASKAP uses the resources of the Pawsey Supercomputing Centre. Establishment of ASKAP, the Murchison Radio-astronomy Observatory and the Pawsey Supercomputing Centre are initiatives of the Australian Government, with support from the Government of Western Australia and the Science and Industry Endowment Fund. We acknowledge the Wajarri Yamatji people as the traditional owners of the Observatory site.

This project has received funding from the European Research Council (ERC) under the European Union’s Horizon 2020 research and innovation programme (grant agreement no. 679627: FORNAX).

REFERENCES

- Bekki, K., Koribalski, B. S., Ryder, S. D., Couch, W. J. 2005, *MNRAS*, 357, L21
- Bertin, E. & Arnouts, S. 1996, *A&AS*, 117, 393
- Blakeslee, J. P., Lucey, J. R., Barris, B. J., Hudson, M. J., Tonry, J. L., 2001, *MNRAS*, 327, 1004
- Bonamente, M., Swartz, D. A., Weisskopf, M. C., & Murray, S. S. 2008, *ApJ*, 686, L71
- Cannon, J. M. et al. 2015, *AJ*, 149, 72
- Chengalur, J. N., Giovanelli, R., Haynes, M. P. 1995, *AJ*, 109, 2415
- Chromey, F. R. Elmegreen, D. M., et al. 1998, *AJ*, 115, 2331
- da Costa, L. N., Wilmer, C. N. A. et al. *AJ*, 116, 1
- Davé, Romeel, Rafieferantsoa, M. H., Thompson, R. J., & Hopkins, P. F. 2017, *MNRAS*, 467, 115
- English, J., Koribalski, B., Bland-Hawthorn, J., et al. 2010, *AJ*, 139, 102
- Erben, T., Schirmer, M., Dietrich, J. P. 2005, *AN*, 326, 432
- Giovanelli, R. & Haynes, M. P. 1989, *ApJL*, 346, 5
- Haynes, M. P., Giovanelli, R., Roberts, M. S. 1979, *ApJ*, 229, 83
- Haynes, M. P., Giovanelli, R., Martin, A. M., et al. 2011, *AJ*, 142, 170
- Hester, J. A. 2006, *ApJ*, 647, 910
- Janesh, W., Rhode, K. L., Salzer, J. J., Janowiecki, S. et al. 2017, *ApJ Letters*, 837, L16
- Janowiecki, S., Leisman, L., et al. 2015, *ApJ*, 801, 96
- Koribalski, B. S., Staveley-Smith, L., Kilborn, V. A., et al. 2004, *AJ*, 128, 16
- Lee-Waddell, K., Spekkens, K., Haynes, M. P., et al. 2012, *MNRAS*, 427, 2314
- Lee-Waddell, K., Spekkens, K., Cuillandre, J.-C., Cannon, J. et al. 2014, *MNRAS*, 443, 3601
- Lee-Waddell, K., Spekkens, K., Chandra, P., et al. 2016, 460, 2945
- Leisman, L., Haynes, M. P., Janowiecki, S., et al. 2017, *ApJ*, 842, 133
- Matsuoka, Y., Ienaka, N., Oyabu, S., et al. 2012, *AJ*, 144, 159
- Meyer, M. J., Zwaan, M. A., Webster, R. L., Staveley-Smith, L. et al. 2004, *MNRAS*, 350, 1195
- Mullan, B., Kepley, A. A. Maybath, A. et al. 2013, *ApJ*, 768, 194
- Osterloo, T., & van Gorkom 2005, *A&A*, 437, L19
- Osmond, J. P. F. & Ponman, T. J. 2004, *MNRAS*, 350, 1511
- Saponara, J., Koribalski, B. S., Benaglia, P., Fernández López, M. 2018, *MNRAS*, 473, 3358
- Schaye, J. 2004, *ApJ*, 609, 667
- Schaye, J. & Dalla Vecchia, C. 2008, *MNRAS*, 383, 1210
- Schirmer, M. 2013, *ApJSS*, 209, 21
- Serra, P., Koribalski, B., Kilborn, V. et al 2015, *MNRAS*, 452, 2680
- Smart, R. L., & Nicastro, L. 2014, *A&A*, 570, 87
- Sparke, L. & Gallagher, J. S. 2007, *Galaxies in the universe : an introduction*, Cambridge, UK: Cambridge University Press, September 2000, page 21
- White, S. D. M. & Rees, M. J. 1978, *MNRAS*, 183, 341
- Wright, E. L. 2006, *PASP*, 118, 1711